A Computational Modeling Appr the Influence of Hyperthermia Microenvironment

Anna Bottiglieri[1], Rahul Shet[2], Punit Prakash[1]

[1]Department of Electrical and Computer Engineering, Kansas State Univers [2]Department of Radiatio Anderson Cancer Center

Corresponding A

Anna Bottiglieri
aabottiglieri@ksu.edu

Abstract

The biophysical properties of the tumor from normal tissues. A constellation of lack of lymphatic drainage, and elevate penetration of therapeutics into tumors. microenvironmental properties, such as in improvements in drug penetration. In this can provide insight into the interplay be tumor microenvironment and can guide the that test the bioeffects of local hyperth

This paper describes a step-by-step work partial differential equations describing and fluid dynamics. The main objective i delivered by a bipolar radiofrequency dev tumor. The system of mathematical express bioheat transfer, and interstitial fluid in the distribution of the interstitial f intervention.

Citation

Bottiglieri, A., Shet Computational Modelin Investigate the Influ on the Tumor Microenv J. Vis. Exp. (202), e65870, doi (2023).

Date Published

December 1, 2023

DOI

10.3791/65870

URL

jove.com/video/658

Introduction

Elevated interstitial fluid pressure (IFP) is a hallmark of solid tumors[1]. The leakage of fluid (TME), ... hyperpermeable blood vessels ... of fluid due to compressed ... lymphatics[1,2,3] in concert with other ...

(renal cell carcinoma) compa[illegible] tissue[2]. High IFP is responsible [illegible] flow toward the margin of t[illegible] cells, infiltrated cells, an[illegible] to shear stress[1,4]. Mechano-biological [illegible] an immunosuppressive TME, f[illegible] endothelial sprouting, which s[illegible] cell migration and invasion, [illegible] (TGF-β) expression,[7,8,9] and stroma[illegible] of the immuno[illegible] infiltration) to external sti[illegible]

Several studies have explored energy-based therapies with the intent of decreasing IFP, including low-[illegible] ultrasound, high-intensity focused [illegible] fields, and thermal therapies[5,10,11]. [illegible] in the range of 40-43 °C, res[illegible] has been shown to increase tumor [illegible] thus contribute to expanding t[illegible] vascular pressure by facilitat[illegible] of interstitial fluid[11,12]. Some recent studies [illegible] potential of hyperthermia to reduce IFP [illegible] to facilitate the distribution of drug [illegible] a tumor[13,14]. These studies also s[illegible] infiltration following hyperthermia compared to no treatment control groups[13].

Figure [illegible] shows the computational [illegible] to calculate thermally induc[illegible] [illegible] normal tissue.

The promising results from [illegible] motivate further studies [illegible] approaches to advance the understanding of [illegible] parameters within the TME [illegible] interventions[4,15,16,17]. Results from computational models [illegible] can complement experimental studies [illegible] the cause-effect relationship of [illegible] (or other external energy sources) [illegible] can be particularly instructive [illegible] measuring spatial variations in IFP with catheter- and nee[illegible]

movement of the interstitial fluid through the extracellular solid matrix[16,17,21].

From the poroelasticity theory, the stress tensor **S** (Pa) (equation [**1**]) is the combination of the elastic term describing the change in volume of the solid component relative to the initial conditions, and a porous term describing the stress induced by the hydrostatic pressure of the fluid component.

$$\boldsymbol{S} = \boldsymbol{S}_{elastic} + \boldsymbol{S}_{porous} = (\lambda e \boldsymbol{I} + 2\mu \boldsymbol{E}) - P_i \quad (1)$$

Where, λ, μ (Pa) are the Lamé parameters, ***E*** is the strain tensor, *e* is the volumetric strain tensor, P_i (Pa) is the interstitial fluid pressure (***I*** is the identity matrix). Steady-state conditions are assumed for the solid component under poroelastic stress, which means that the stress tensor components are orthogonal, $\nabla \cdot \boldsymbol{S} = 0$.

Figure 2 shows the system of mathematical equations implemented in the described poroelastic model and the interplay between the components of the presented multi-physics model. The workflow of the computational simulations includes:

Electrical problem equations. The solution of the electrical problem equations provides the time-averaged RF heat source Q (Joule heating). To this end, a quasi-static approximation to Maxwell's equations is used to calculate the distribution of the time-averaged electric field **E** (V/m) (**Figure 2**, block 1).

Thermal problem equations. The solution of the Pennes bioheat equation (**Figure 2**, block 2) provides the spatial and temporal variation of the temperature T (°C) as a result of the heat source (Q) linked to the absorbed electromagnetic energy, the passive heating linked to the thermal conduction of the tissues ($\nabla \cdot k(T)\nabla T$), and the heat sink effect of the tissue blood perfusion ($cW_b(T)$ (T - T_b)). The heat sink term approximates the heat exchange between the blood flowing in the microvasculature and adjacent tissue where electromagnetic power is absorbed. The heat transfer equation also includes the advection term ($\rho c \boldsymbol{u}(P_i) \cdot \nabla T$), which describes the change in the temperature caused by the movement of interstitial fluid through the extracellular matrix of the poroelastic model. However, this term has a negligible impact on the temperature profile compared to the other mechanisms responsible for the temperature change.

Fluid-dynamic problem equations. The conservation of mass equation (**Figure 2**, block 3) combined with Darcy's law (**Figure 2**, block 4) gives as an output the spatial and temporal variation of the interstitial fluid pressure P_i resulting from the balance between the source ($L_{p_c}\frac{S}{V} \cdot (P_v - P_i)$) and the sink ($L_{p_L}\frac{S}{V} \cdot (P_L - P_i)$) of the fluid. The transient pressure term on the left side of the mass conservation equation, $\left(\frac{1}{2\mu+\lambda}\frac{\partial P_i}{\partial t}\right)$, describes the rearrangement of the fluid and solid components in the poroelastic material. This is caused by the variation of the interstitial fluid pressure, P_i, driven by the variation of the vascular pressure P_v as a function of the temperature.

The difference between the vascular pressure (P_v) and the interstitial fluid pressure (P_i) is the source of the fluid that flows through the extracellular matrix. The sink term is linked to the pressure difference between the lymphatic vessels (P_L) and the interstitial space (P_i). In normal tissue, the pressure in the lymphatic vasculature (~ -6-0 mmHg) is up to two-fold lower than the interstitial fluid pressure[13]. This pressure difference ensures the efficacy of the lymphatic vessels to drain the excess of the fluid extravasating from the wall of blood vessels

into the interstitium. For the model presented here, we neglected the contribution of the lymphatic system[4,16,22].

Mathematical expressions from Equations (2) to (5) are used to describe the temperature dependence of the electrical and thermal conductivity and of the blood perfusion[23,24]. Two different mathematical models are used to describe the temperature dependence of the blood perfusion in the normal and tumor tissue domains, respectively[24,25]. The models show that the blood perfusion increases with temperature up to nine times compared to the baseline value in the normal tissue and only approximately two times the baseline value in the tumor domain. For both models, the increase in the blood perfusion is limited to temperatures within the mild hyperthermia range (below 45 °C). It is worth mentioning that the mathematical expressions, Equations (4) and (5), do not fully describe the mechanisms underlying the temperature-dependent changes in the blood perfusion in the two different types of tissue. However, they help represent the limited perfusion that typically characterizes the tumor microenvironment compared to normal tissues.

$$\sigma(T) = \sigma_0\left(e^{0.015\cdot(T-37°C)}\right) \quad (2)$$

$$k(T) = k_0 + 0.0008\cdot(T-37°C) \quad (3)$$

$$W_{normal}(T) = \begin{cases} W_0 + 2.28\cdot e^{-\frac{(T-45)^2}{6.5}}, & 37°C \le T < 43°C \\ 4.64 - 0.75\cdot(T-45)^2, & 43°C \le T < 46°C \\ W_0 + 2.28\cdot e^{-\frac{(T-45)^2}{6.5}}, & T \ge 46°C \end{cases} \quad (4)$$

$$W_{tumor}(T) = \begin{cases} W_0 + 0.37\cdot e^{-\frac{(T-42)^2}{6.5}}, & 37°C \le T < 42°C \\ W_0\cdot(T-43)^2 + 0.23, & 42°C \le T < 43°C \\ 0.18, & T \ge 43°C \end{cases} \quad (5)$$

$$P_{v_{normal}}(W_{normal}) = P_{v_0} - \left.\frac{\frac{W(T)}{\rho_b}}{\left(L_{p_c}\frac{S}{V}\right)}\right|_{normal} \quad (6)$$

$$P_{v_{tumor}}(W_{tumor}) = P_{v_0} - \left.\frac{\frac{W(T)}{\rho_b}}{\left(L_{p_c}\frac{S}{V}\right)}\right|_{tumor} \quad (7)$$

In this study, we used (Equations 6 and 7) the dependence of the vascular pressure as a function of ... in the normal and tumor tissue[26]. First, ... Equation (4) and (5) ... the blood flow rate ... the blood perfusion and the ... between blood inflow and outflow ... increase in the blood flow rate ...[3]: ... resistance (L_p) ... conductivity ... the pressure difference ... pressure increase ... temperature range below 45 °C ... the temperature-dependent models (Equations 4 and 5) ...

The implementation of the ... (Figure 2) and the temperature-dependent models are described in detail ... material properties and their ... (i.e., at body temperature) ... Table 1. See Table of Materials for details about C... installed on a computer used ... protocol. The electrical problem ... DC module; bioheat transfer w... physics; and the fluid-dynami... the Mathematics interface.

Protocol

1. Build the model of a bi... system

1. Preliminary steps to set th...

1. Launch COMSOL Multiphysics | Model Wizard.
2. Select 3D as Space Dimension.
3. Select AC/DC Physics module | Electric Fields and Currents | Electric Currents.
4. Select Heat Transfer module | Heat Transfer in Solids.
5. Select Mathematics module | PDE interfaces | Coefficient Form PDE.
6. Select Study | Time-dependent | Click Done.
7. Once the Comsol working space appears:
    1. Select Multiphysics | Electromagnetic Heating. With this step, the electromagnetic power loss density is automatically coupled as the heat source for the bioheat transfer equation.
    NOTE: If Multiphysics does not appear automatically, manually specify the electromagnetic heat source (shown in COMSOL as Volumetric loss density). For more details on how to add the heat source, see 'Physics' section, step 2 'Set up the thermal problem'.
    2. Select Study from the top ribbon | Study Steps | Frequency Transient.

2. Define the geometries. From the top ribbon, select Geometry, then:
    1. Define two cones with the dimensions listed in Table 2.
    2. Position the cones at the distance indicated in Table 2 (spaced $d_{inter-el}$ apart). These two cones will model the two hypodermic needle[s of the] bipolar RF system.
    3. Duplicate the two previo[us] insulation of the needles according to the dimensions in Table 2.
    4. Select a cylinder (diameter d_m, height h_m) to model the bulk of muscle 0, y = 0). The values of Table 2.
    5. Select a cylinder (diameter d_s, height h_s) to model the thin layer of s = 0, y = 0). The values o in Table 2.
    6. Select a sphere (diameter d_t) to model subcutaneous tumor placed = 0). The size of the tum Table 2.
    7. To facilitate the selecti following steps of the pr following:
        1. From the Geometry ribbon, Select operations | Form Compo
        2. Select all the thermal conductive part of the composite geometry.
        3. Repeat the same proce composite domains for geometries.

3. Define the properties of th

NOTE: The following steps des implement the mathematical Equations (2)–(7)

1. From Component, node right-click to Definitions.

2. Under Functions, select Analytic.

   1. Specify the name of the function (e.g., k_muscle or sigma_muscle) and type the mathematical expression (Eq. 2).

   2. Specify temperature as argument (T).

   3. Specify the Units of the function (S/m in the case of electrical conductivity).

   4. Repeat the previous steps to implement Eq. 3, modifying the unit accordingly (i.e., W/(m·K) for thermal conductivity).

   5. Specify the unit of the argument: K (kelvin). Under Plot Parameters, specify the range of values of the function argument (i.e., temperature). To follow this protocol, use a range of 33-100 °C (306.15-373.15 K).

   6. Repeat the previous steps from 1 to 5 to add the temperature-dependent functions of electrical (Eq. 2) and thermal conductivities (Eq. 3) for each tissue modeled (i.e., muscle, skin, and tumor) using the nominal values listed in Table 1 (normal tissue refers to both muscle and skin).

3. Under Functions, select Piecewise to implement Equations (4)-(7).

   1. Specify the name of the function.

   2. Specify temperature (T) as the argument of the function.

   3. Type the mathematical ... temperature interval co... (4)-(7).

   4. Repeat the previous ste... the temperature-depende... perfusion and vascular ... model using the nominal ... Table 1 (normal tissue refers ...

4. Assign material properties ...

   1. From the component, select Materials.

   2. Select blank material ... normal ti... tumor tissue, ... stainless ... PTFE ...

   3. Enable manual selection of the geometric entity corresponding to the material.

      1. Normal tissue is assoc... modeling muscle and ski...

      2. Tumor and blood tissues ... the tumor geometry.

      3. PTFE material is ass... geometries modeling the ...

      4. Stainless steel materia... cone geometries modelin... active needles.

   4. For the temperature-dependent ... thermal conductivity[2,3], ... the function and the argument (i.e., T), tha... appears in the Definitions node.

   5. For the material proper... temperature, refer to the ...[27] listed in Table 1.

NOTE: We rely on the poroelastic theory[16,17,26] to calculate the pressure. The following steps show how the properties of a porous material can be assigned to a specific domain.

6. From Materials, select Materials | Porous Material.

7. Right-click on Porous Material and select Fluid and Solid components. Under Fluid properties, select Blood (defined in previous steps). Under Solid properties, select Tumor (defined in the previous steps). Specify the porosity volume fraction defined (Table 1).

8. Enable manual selection of geometric entity corresponding to the tumor material. To follow this protocol, assume that only the tumor region is a poroelastic domain.

5. Meshing

1. Under Mesh node, select Size and select a predefined Fine mesh.

2. Add Free Tetrahedral Mesh under Mesh node. This step allows for a refined mesh in the critical areas.

NOTE: For this model, we identified the edges of the tumor and the distal end of the hypodermic needle models as critical areas.

3. Select the geometries and customize the maximum (0.25 mm) and minimum element size in a way that the smallest component (e.g., the tip of the needle) is discretized by at least four meshing elements (complete mesh consists of 1,487,828 elements).

2. Physics

1. Set up for the electrical pr

NOTE: The following steps pro
to set the parameters to
distribution (Figure 2, block 1) that
radiofrequency heat source

1. Right-click on Electric Currents

2. For the electrical boundaries shown in Figure 3, set Terminal and Ground boundaries.

1. For Terminal, manually select the proximal end (on the top) of the needle. The identified needle will

2. Under Terminal, select Power and specify value according to the des
To follow this protocol, 0.5 W for com
hyperthermia based on ex vi
experiments[20].

3. Select Ground and manually proximal surface end needle. The needle will act as a r
returning path of the e

4. Apply electrical external surface of the

2. Set up for the thermal probl

NOTE: The following steps sh
the temperature-dependent
(Equations 4 and 5) in the
model the heat sink caused

1. Select Heat Transfer in Solids and 33 °C as the initial value of the tempera

2. To model the heat-sink effect due to the blood flow, right-click Heat Transfer, and select Heat Source domain, and select the geometry where the heat sink effect should be considered (i.e., tumor and normal tissue). Select General Source | User defined where the expression for the heat sink can be typed.

3. For the thermal boundary condition, see Figure 3B, right-click Heat Transfer, and select Heat Flux as boundary condition, and specify the external surfaces to which the heat flux is applied. Select Convective heat flux. For the heat transfer coefficient, use h = 15 W/(m^2K) to model the mechanism of natural heat exchange between the skin and the air[28]. Specify the external temperature T_{ext} = 20 °C to model the ambient temperature in the laboratory environment.

3. Setup for the fluid-dynamics problem

NOTE: The following steps describe how to implement the conservation of mass equation (Figure 2, Block 3) and how it can be linked to the variation of temperature.

1. Select Coefficient Form PDE, modify the Pressure dependent variable. At this stage, the unit Pascal (Pa) is automatically assigned.

NOTE: Once the simulation is computed, the results can be displayed and/or exported using the unit of choice. We present the results using mmHg unit for consistency with the literature (see the representative results section).

2. Specify fluid conductivity unit as source term quantity:

3. Define the domain to model the interstitial fluid pressure ... [illegible]

4. Right-click Coefficient Form PDE ... [illegible] ... select Coefficient Form domain. Spe[cify the] geometrical domain to which the eq[uation] ... (tumor). Repeat the same st[eps for the] remaining normal tissue(s) to which PDE should be applied.

5. For the tumor model, specify th[e] coefficients and terms of the conservation of mass equation (Figure 2, Block 3): diffusion coefficient c (Table 1); damping coefficient $a = \frac{1}{2\mu+\lambda}$; source term $f = \left(L_{p_c}\frac{S}{V}\right)\cdot(P_v(T)-P_i)$. For the tumor, ... the contribution of the l[ymphatic] ... coefficient ... equal to zer[o].

6. For normal tissues, modify the following coefficients as illustrated in Figure 2 Block 3: diffusion coefficient c (Table 1); damping coefficient $a = \frac{1}{2\mu+\lambda}$; source term $f = \left(L_{p_c}\frac{S}{V}\right)\cdot(P_v(T)-P_i) + \left(L_{p_L}\cdot\frac{S}{V}\right)\cdot(P_L-P_i)$. To consider normal tissue ... tissue, consider the con[tribution of the lymphatic] system. Set all other coe[fficients] ...

7. To create the link with t[he thermal] simulation, vascular pressure ... function of temperature by means of perfusion variable (see Eq 6 and 7).

8. Right-click Coefficient Form PDE and select Initial Values ... geometrical ...

(tumor) and repeat the same step for the normal tissue (normal tissue). Specify T_0 of tumor and normal tissue according to the values listed in Table 1.

9. For the boundary conditions related to the fluid-dynamic study, Figure 3C, right-click on Coefficient Form PDE and select Dirichlet Boundary condition. Select the external surface of the normal tissue domain and assign the p_0 value corresponding to the normal tissue (Table 1).

3. Run the simulations and display the results

NOTE: As a final step before computing, specify the time (simulating the duration of the procedure) and the frequency.

1. Select Frequency-Transient in the Study node.
   1. Specify the time unit (s).
   2. From Output Times, select range (on the right side) and specify 0 s as start, 5 s as step, and 900 s as stop.
   3. Set the frequency as 500e3 Hz.
2. Select Compute to run the simulations.
3. For the visualization of the results, select Data sets under the Results node.
   1. Right-click Cut plane and define the plane to use to visualize 2D distributions (e.g., y = 0).
   2. Right-click Cut point 3D and select the volume to display the variation of a parameter across time.
4. From Results on the top ribbon,
   1. Select 2D plot group to visualize two-dimensional distribution (e.g., temperature) on one of the pla... steps above.
   2. Select 1D plot group to visualize 1D (e.g., pressure across the time) in the points identified in the ...

NOTE: The time to run the settings described in thi... is 2.5 h (

Representative Results

The homogeneous distribution ... pressure within the tumor and ... (0-3 mmHg) at the periphery ... Figure 4 and Figure 5 show the initial ... min) of temperature (A), int... fluid velocity (C). Before st... temperature is 33 °C, the va... within the tumor is approxima... to 3 mmHg at the periphery. ... during in vivo experiments (a drop in ... 37 °C is often an effect of t...[19]).

The gradient of pressure bet... and the periphery influences ... Figure 4 and Figure 5). Darcy's law descri... relationship between the int... fluid velocity by means of t... (K_i). Before heating, fluid ve... within the tumor and abruptl... approaching the tumor's peri... of the interstitial fluid ve... within the range of those re...

(µm²/s)[12]. Translating the init... pressure and velocity into a ... is intratumorally injected, ... toward the periphery of the ... to escape from the tumor.

Figure 4A and Figure 5A show the gradient of the temperature resulting from the absorbed electromagnetic power in the tissue model (Joule's effect) at the end of the procedure (t = 15 min). Simulating a constant applied power level of 0.5 W for 15 min, mo... (~723 mm³) reached temperatures ... hyperthermia (40-43 °C). The ... the spatial distribution ... Figure 4B and Figure 5B ... fluid velocity (Figure 4C and Figure 5C) in response to the gradient ... to the initial conditions, the ... decreases from 9 mmHg in the ... at the edge. Fluid velocity ... the entire tumor domain, inc...

After 15 min of the simulated heating with 0.5 W applied power, the temperature in the region of the tumor closest to the needle exceeds 45 °C (Figure 4A and Figure 5A).

The mathematical ... of both fluids (Equations 4 and 5) model ... the increase in the temperature up to 42 °C ... tumor, it is likely ... vascular pressure-the driving pressure-starts increasing wh... 42 °C according to the mathe... to describe the relationship ... blood perfusion (Equation 7).

Figure 6 shows ... of the tumor volume ... fluid pressure over time at ... results ... 3 cm from ... corresponds to the ... interstitial fluid pressure ... end of the heating, this reg... values of the fluid pressure ... However, ... surrounding the tumor ... 0 mmHg ... decrease ... 0.2 µm/s ... Overall, the numerical ... provides insight into the li... profiles and the rate of heat...

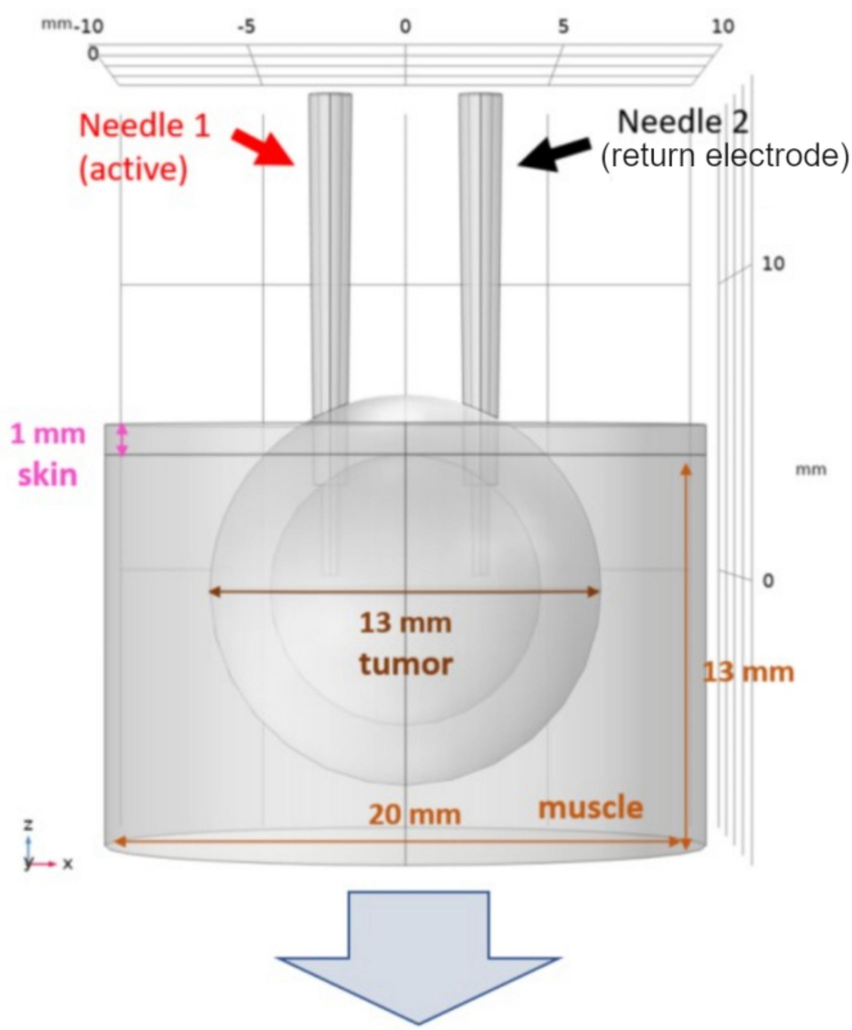

Figure 1: Geometry for numerical model of a small-animal tumor. The active and return electrodes are placed in the tumor domain, rep... Please click here to view a larger version of this figure.

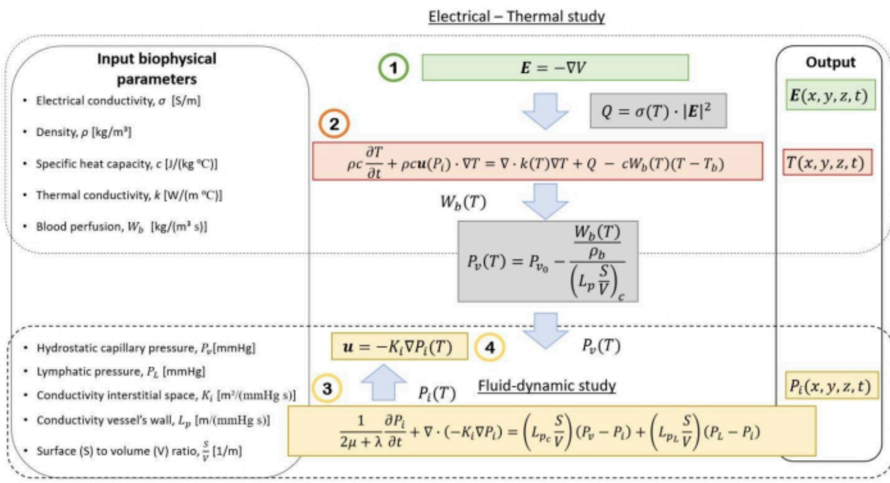

Electrical – Thermal study
Input biophysical parameters
• Electrical conductivity, σ [S/m]
• Density, ρ [kg/m³]
• Specific heat capacity, c [J/(kg °C)]
• Thermal conductivity, k [W/(m °C)]
• Blood perfusion, W_b [kg/(m³ s)]
1
$E = -\nabla V$
$Q = \sigma(T) \cdot |E|^2$
2
$\rho c \frac{\partial T}{\partial t} + \rho c \mathbf{u}(P_i) \cdot \nabla T = \nabla \cdot k(T) \nabla T + Q - c W_b(T)(T - T_b)$
$W_b(T)$
$P_v(T) = P_{v_0} - \frac{\frac{W_b(T)}{\rho_b}}{\left(L_p \frac{S}{V}\right)_c}$
Output
$E(x, y, z, t)$
$T(x, y, z, t)$
$P_i(x, y, z, t)$
• Hydrostatic capillary pressure, P_v [mmHg]
• Lymphatic pressure, P_L [mmHg]
• Conductivity interstitial space, K_i [m²/(mmHg s)]
• Conductivity vessel's wall, L_p [m/(mmHg s)]
• Surface (S) to volume (V) ratio, $\frac{S}{V}$ [1/m]
$\mathbf{u} = -K_i \nabla P_i(T)$
4
$P_v(T)$
3
$P_i(T)$
Fluid-dynamic study
$\frac{1}{2\mu + \lambda} \frac{\partial P_i}{\partial t} + \nabla \cdot (-K_i \nabla P_i) = \left(L_{p_c} \frac{S}{V}\right)(P_v - P_i) + \left(L_{p_L} \frac{S}{V}\right)(P_L - P_i)$

Figure S2: Schematic representation of the numerical protocol s parameters between the physics. The parameters were used to calculate E (V/ m), temperature - T (°C), and interstitial fluid pressure radiofrequency system model. The values and descriptions o Table A1. A quasi-static approach (block 1) calculates the electrical field (E). The Bioheat equation (block 2) is used to calculate the temperature (T). Consecutively, block 3 ... equation ... interstitia (block 4) calculates the fluid velocity (u) linked to the gradient of interstitial the tumor domain. Please click here to view a larger version of thi

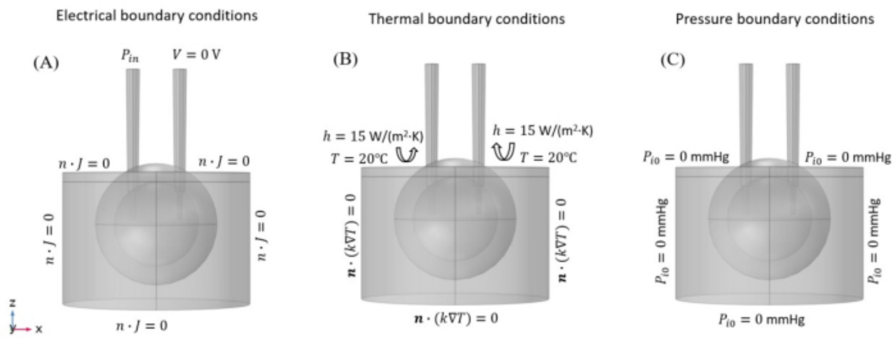

Figure 3: Boundary conditions used in the computational model … simulation. (A) Electrical boundary conditions simulating null e… electrode (P_{in}) and return electrode (0 V). (B) Thermal boundary conditions simulati… the muscle and the effect of the … (C) Fluid-dynamic boundary conditions … normal values of the interstitial fluid pressure in… Please click here to view a larger version of this figure.

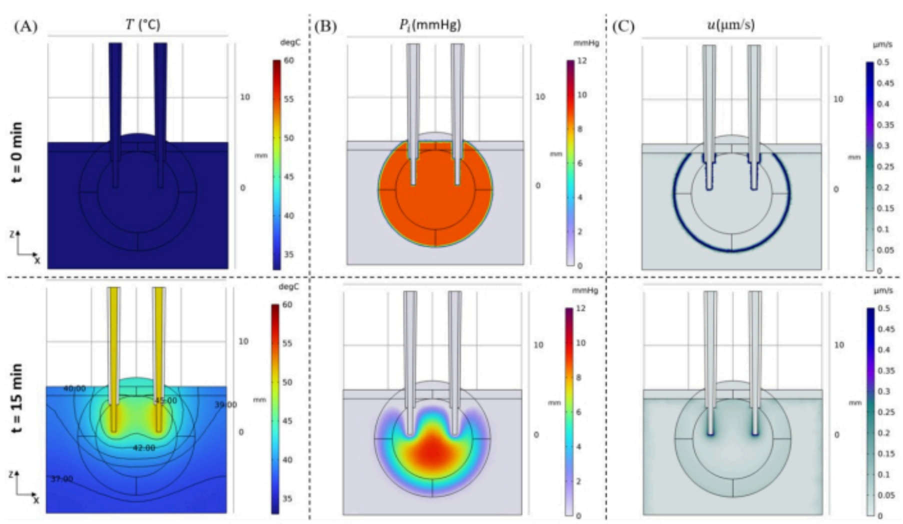

Figure 4: Distributions shown in a… (A) Temperature, (B) … (C) … fluid velocity before starting the heating (first line) an… radiofrequency system operating at 500 kHz. One needle is … to close the electric current path. Please click here to view a larger version of this figure.

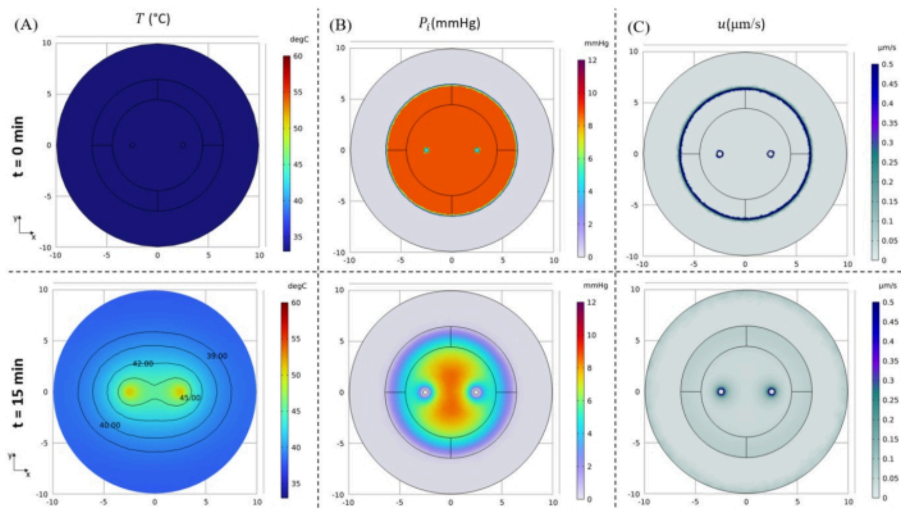

Figure 5: Distributions shown in a plane. (A) Temperature, (B) interstitial ... and (C) fluid velocity before starting the heating (first line ... bipolar radiofrequency system operating at 500 kHz. One ne... is used to close the electric current path. Please click here to view a larger vers...

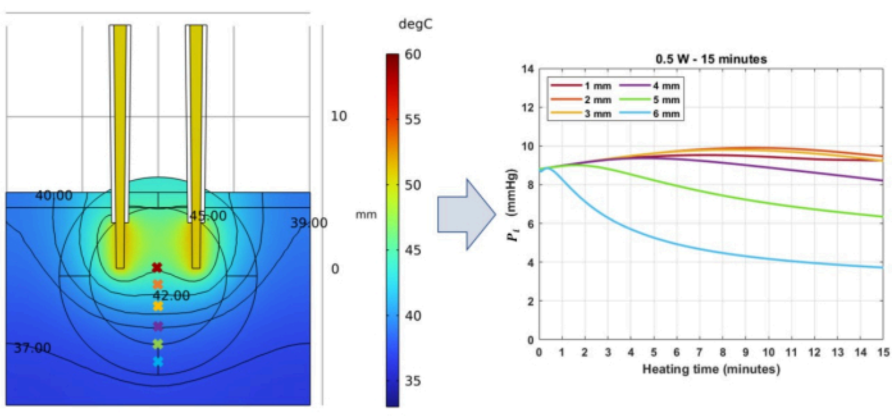

Figure 6: Temperature distribution and associated ... (Left) ... thermal ... min. (Right) Interstitial fluid pressure across the time ... direction from the heating source to the periphery of the ... a different temperature value visible in the left panel. Please click here to view a larger ...

Table 1: List of parameters, including description, values, nominal values, and related numerical references. *For the tumor, the ... indicating the effect of the ... Please click here to download this Table.

Table 2: Geometrical parameters and related values used for modeling the system. Two hypodermic needles placed in a tumor resembling an experimental scenario with a separation distance of 5 mm, and the tumor embedded in a muscle tissue, and ... Please click here to download this Table.

Discussion

We present a computational modeling protocol to couple transient electric-thermal simulations with fluid-dynamic simulations to study the impact of RF-hyperthermia on thermal and interstitial fluid pressure profiles in tumors. A key aspect is in the building of a numerical workflow capable of capturing the relationship existing between temperature and vascular pressure, which in turn drives the changes in interstitial fluid pressure.

We used the relationship between vascular pressure and blood perfusion to model the temperature-dependent vascular pressure parameter in the conservation of mass equation (Figure 2). In the range of mild hyperthermia temperatures (40-43 °C), the blood perfusion term increases from the baseline (T = 37 °C). At temperatures higher than 43 °C, the blood perfusion decreases, and the vasculature stasis occurs when ablation temperatures are approached (≥50 °C). We implemented temperature-dependent blood perfusion models (Equations 4 and 5) for both tumor and muscle geometries. As a result, the dependence of the vascular pressure on the temperature has been established through the blood perfusion term. The mathematical descriptions o…

In this study, we implemented ... dependent system[24]. An alternative approach this step could be b… variation of the blood perfus… the mathematical function des… across the temperature can be… For this study, we assumed a… [13] meaning that 70% of the tissu… phase and 30% is void space (… The degree of porosity varie… its variability may affect t… and pressure. As a first app… describing the thermal dilat… the poroelastic tumor domain… should be considered in a fu… structural changes of the so… The increase in the volume of… thermal dilation may enhance… affect the gradient of the in… tumor. Further study is requi… which the dilation of the ext… biomechanical parameters of t…

Finally, in this protocol, … system using 23 G hypodermic… in vivo experimental small ani… numerical workflow can be i… effects of hyperthermia by o… temporal energy-density profi… temperature that determines… tissue. In the case of very… relatively short time (less t…

pressure gradients decreases. In other words, with the rise of the temperature, the IFP profile is perturbed.

Recent studies have shown that the potential of interventional thermal procedures designed to intentionally modulate biophysical characteristics of the tumor microenvironment rather than ablate tumor tissue, may yield favorable ramifications on local and systemic tumor immunity[3,30,31,32]. In this context, numerical simulations coupling electrical and thermal physics with fluid dynamics could provide further insights into how energy-based interventions perturb tumor biophysical parameters such as IFP. Of note, the methods used to measure interstitial fluid pressure techniques (i.e., wick in needle, piezoelectric probes) providing quantitative information only for a limited number of measurement points in the tissue. Computational models may provide a means to complement the measurements to assess IFP changes across the space.

In addition to IFP, the increase in blood perfusion following a mild increase in temperature has the potential to modulate other biophysical hallmarks of the tumor microenvironment, including the level of oxygenation[3,33,34]. A number of preclinical studies demonstrated that an increase in blood perfusion in the region where the temperature is between 3[illegible] °C and 45 °C correlates with a shift to hypoxic to normoxic conditions that could increase the tumor control probability to 100% for radiotherapy[34].

The numerical assessment of the spatial-temporal variation of the pressure with the temperature could help support the findings of the experimental studies. Imaging techniques including computer tomography, ultrasonography, and magnetic resonance, provide real-time information, for example, about the position of the needles/catheters in

the tumor, the surrounding ... perfusion, and the local ... drug/contrast agent. In the ... studies, numerical models cou... the data that imaging techni... computational models can be ... distribution of the pressure... protocol adopted and eventual... drug systemically delivered ... modeling informed approach co... of imaging sessions and the ... procedures.

The numerical model provide... simplified ... Besides ... including hydraulic conductivity ... Computational models may ... complex ... the increase in temperature. ... model we presented in this s... analyses to identify the biop... a significant effect on the o... of the vasculature within the... insight into the impact of t... profiles. The workflow here ... can be refined, including (fo... derived from experimental stu...

Disclosures

The authors have no conflicts ...

Acknowledgments

The study was supported by grants from the National Science Foundation (no. 2039014) and the National Cancer Institute (R37CA269622).

References

1. Nia, H. T., Munn, L. L., Jain, R. K. Physical traits of cancer. Science. 370 (6516), 546-556 (2020).
2. Heldin, C.-H., Rubin, K., Pietras, K., Östman, A. High interstitial fluid pressure - an obstacle in cancer therapy. Nature Reviews Cancer. 4 (10), 806-813 (2004).
3. Jain, R. K. Determinants of tumor blood flow: a review. Cancer Research. 48, 2641-2658 (1988).
4. Stylianopoulos, T., Munn, L. L., Jain, R. K. Reengineering the physical microenvironment of tumors to improve drug delivery and efficacy: from mathematical modeling to bench to bedside. Trends in Cancer. 4 (4), 292-319 (2018).
5. Sheth, R. A., Hesketh, R., Kong, D. S., Wicky, S., Oklu, R. Barriers to drug delivery in interventional oncology. Journal of Vascular and Interventional Radiology. 24 (8), 1201-1207 (2013).
6. Chauhan, V. P., Stylianopoulos, T., Boucher, Y., Jain, R. K. Delivery of molecular and nanoscale medicine to tumors: transport barriers and strategies. Annual Review of Chemical and Biomolecular Engineering. 2 (1), 281-298 (2011).
7. Li, R. et al. Interstitial flow promotes macrophage polarization toward an M2 phenotype. Molecular Biology of the Cell. 29 (16), 1927-1940 (2018).
8. Stine, C. A., Munson, J. M. ... under differential interst... Biophysica. 2 (1), 16-33 (2022).
9. Provenzano, P. P. et al. ... the stroma ablates physica... pancreatic ductal adenocarc... Cancer Cell. 21 (3), 418-429 (2012).
10. Pal, K., Sheth, R. A. E... immune microenvironment th... interventions. Cancers. 15 (1), 196 (2022...
11. Dunne, M., Regenold, M., A... alter tumor physiology and ... therapy efficacy. Advanced Drug Deliv... 163-164, 98-124 (2020).
12. Vaupel, P. et al. From lo... to improved tumor oxyge... mechanisms critically invo... radio-immunotherapy. Cancers. 15 (5), 1394 (...
13. Stapleton, S. et al. Radi... the delivery and efficacy... modulating intratumoral ... ACS Nano. 12 (8), 7583-7600 (2018).
14. Li, Q., Zhou, Y., Zhang, ... X. Radiofrequency hyperthe... delivered oncolytic immuno... adenocarcinoma. Cardiovascular and ... Radiology. 45 (12), 1812-1821 (202...
15. Mpekris, F. et al. Combi... normalization strategies ... immunotherapy. Proceedings of the ... of Sciences. 117 (7), 3728-3737 (202...

16. Netti, P. A., Baxter, L. T., Boucher, Y., Skalak, R., Jain, R. K. Time-dependent behavior of interstitial fluid pressure in solid tumors: implications for drug delivery. Cancer Research. 55, 5451-5458 (1995).

17. Andreozzi, A., Iasiello, M., Netti, P. A. Effects of pulsating heat source on interstitial fluid transport in tumour tissues. Journal of The Royal Society Interface. 17 (170), 612-626 (2020).

18. Leunig, M. et al. Interstitial fluid pressure in solid tumors following hyperthermia: possible correlation with therapeutic response. Cancer Research. 52, 487-490 (1992).

19. Muñoz, N. M. et al. Immune modulation by molecularly targeted photothermal ablation in a mouse model of advanced hepatocellular carcinoma and cirrhosis. Scientific Reports. 12 (1), 14449 (2022).

20. Bottiglieri, A. et al. RF-hyperthermia to modulate the interstitial fluid pressure: an innovative approach. 38th Annual Society for Thermal Medicine Meeting (2023).

21. Baxter, L. T., Jain, R. K. Transport of fluid and macromolecules in tumors. I. Role of interstitial pressure and convection. Microvascular Research. 37 (1), 77-104 (1989).

22. Stapleton, S. et al. A mathematical model of the enhanced permeability and retention effect for liposome transport in solid tumors. PLoS ONE. 8 (12), 1-10 (2013).

23. Rossmann, C., Haemmerich, D. Review of temperature dependence of thermal properties, dielectric properties, and perfusion of biological tissues at hyperthermic and ablation temperatures. Critical Reviews in Biomedical Engineering. 42 (6), 467-492 (2014).

24. Song, C. W., Lokshina, A., Rhee, J. G., Patten, M., Levitt, S. H. Implication of blood flow in hyperthermic treatment of tumors. IEEE Transactions on Biomedical Engineering. BME-31 (1), 9-16 (1984).

25. Tompkins, D. T. et al. Temperature-dependent versus constant-rate blood perfusion modelling in ferromagnetic thermoseed hyperthermia: results with a model of the human prostate. International Journal of Hyperthermia. 10 (4), 517-536 (1994).

26. Andreozzi, A., Iasiello, M., Netti, P. A. A thermoporoelastic model for fluid transport in tumour tissues. Journal of The Royal Society Interface. 16 (154), 0030-0046 (2019).

27. Hasgall, P. A. et al. IT'IS Database for thermal and electromagnetic parameters of biological tissues. (2022).

28. Cavagnaro, M. et al. Influence of the target tissue size on the shape of ex vivo microwave ablation zones. International Journal of Hyperthermia. 31 (1), 4… (2015).

29. Munson, J., Shieh, A. Interstitial fluid flow in cancer: implications for disease progression and treatment. Cancer Management and Research. 6, 31… (2014).

30. Muñoz, N. M. et al. Influence of injection technique, drug formulation and tumor microenvironment on intratumoral immunotherapy delivery and efficacy. Journal for ImmunoTherapy of Cancer. 9 (2), e0018… (2021).

31. Swartz, M. A., Lund, A. W. Lymphatic and interstitial flow in the tumour microenvironment: linking mechanobiology with immunity. Nature Reviews Cancer. 12 (3), 21… (2012).

32. Mehta, A., Oklu, R., Sheth, R. A. Thermal ablative therapies and immune checkpoint modulation: can locoregional approaches effect a systemic response? Gastroenterology Research and Practice. 2016, 1-11 (2016).

33. Song, C. W., Park, H., Griffin, R. J. Improvement of tum oxygenation by mild hyperthermia. Radiation Research. 155(4), 515-528 (2001).

34. Dewhirst, M. W., Oleson, J. R., Kirkpatrick, J., Secomb T. W. Accurate three-dimensional thermal dosimetry and assessment of physiologic response are essential for optimizing thermal therapy. Cancers. 14(7), 1701 (2022).